

Modulation of the Local Density of States of Carbon Nanotubes by Encapsulation of Europium Nanowires As Observed by Scanning Tunneling Microscopy and Spectroscopy

Terunobu Nakanishi,[†] Ryo Kitaura,[†] Takazumi Kawai,^{‡,§} Susumu Okada,[§] Shoji Yoshida,^{||} Osamu Takeuchi,^{||} Hidemi Shigekawa,^{||} and Hisanori Shinohara^{*,†,||}

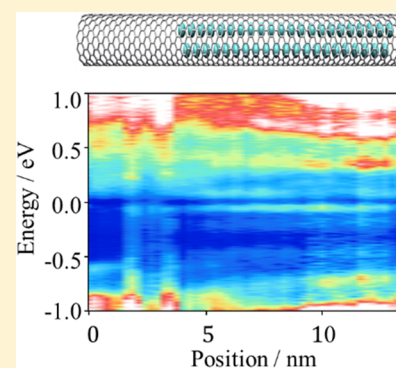
[†]Department of Chemistry & Institute for Advanced Research, Nagoya University, Nagoya 464-8602, Japan

[‡]Security Research Laboratory, NEC Corporation, 1753 Shimonumabe, Nakahara, Kawasaki, Kanagawa 211-8666, Japan

[§]Graduate School of Pure and Applied Sciences and ^{||}Faculty of Pure and Applied Sciences, University of Tsukuba, Tsukuba, Ibaraki 305-8571, Japan

Supporting Information

ABSTRACT: Modulation of the local density of states of single-wall carbon nanotubes (SWCNTs) is induced by the encapsulation of europium nanowires (EuNWs). The observation of these modulated density of states using scanning tunneling microscopy/spectroscopy combined with density functional theory calculations is reported. The electronic modulation of SWCNTs by encapsulation of EuNWs is revealed as a Fermi level shift, band gap reduction, and the emergence of localized states in the gap. The present results show that the electronic interaction between EuNWs and SWCNTs is much stronger than that previously reported for nanomaterials encapsulated in SWCNTs.



1. INTRODUCTION

One-dimensional (1D) materials have been studied because of their fundamental importance and interests in nanometer-scale materials science together with potential applications in nanoelectronic devices for charge, spin, and heat transport. Single-wall carbon nanotubes (SWCNTs) are 1D materials that have excellent mechanical and electronic properties^{1,2} for potential applications in various fields. In particular, the band gap of SWCNTs can be varied from 0 to 1.5 eV, depending on the geometrical structure of the SWCNTs, and their electrical conductivity can be metallic or semiconducting according to their chirality.^{3,4}

SWCNTs are 1D hollow structures that enable the synthesis of materials restricted to wire structures encapsulated in the SWCNTs. One-dimensional materials encapsulated in SWCNTs are novel hybrid materials that should exhibit specific low dimensional properties and structures. Various 1D structures inside carbon nanotubes (CNTs), such as molecular arrays,^{5,6} long linear carbon chains,^{7–9} metal complex nanowires,^{10–13} and metal atomic nanowires (NWs),^{14–16} have been synthesized during the past couple of decades. Metal NWs that are normally synthesized by a direct nanofilling method originally developed in our laboratory form 1D ultrathin NWs of 1 nm to several nanometers in diameter.¹⁶ The properties of 1D ultrathin NWs, such as their structure, optical, electrical, and magnetic properties,^{15,16} are different from those of the bulk crystals. NWs are typically mechanically fragile and

chemically reactive/unstable under ambient conditions. NWs encapsulated in CNTs (NW@CNTs) are, by contrast, totally stable under ambient conditions and their novel properties can be well-characterized.

Density functional theory (DFT) band structure calculations can explain the properties of NWs from the calculated electronic structure. DFT band structure calculations^{17,18} for metal NWs encapsulated in CNTs have suggested that charge transfer from the metal NWs to the CNTs occurs and that the electronic structure of NW@CNTs cannot be explained as a simple superposition of neutral NWs and CNTs. To understand the basic properties and the structure of NW@CNTs and to elucidate their electronic structure, it is thus important to investigate the interactions exerted between NWs and CNTs.

Scanning tunneling microscopy and spectroscopy (STM/STS) is a powerful method used to obtain information on the electronic local density of states (DOS) near the Fermi level, which dominates the electronic properties of these materials. This technique reveals the electronic structure of CNTs and hybrid CNTs including NW@CNTs. STM studies on C₆₀ peapods,¹⁹ Gd@C₈₂ peapods,^{20,21} and other metallofullerene peapods²² have revealed periodic band gap modulation of CNTs. The band gap modulation in these systems accounts for

Received: April 29, 2017

Revised: July 11, 2017

Published: July 31, 2017

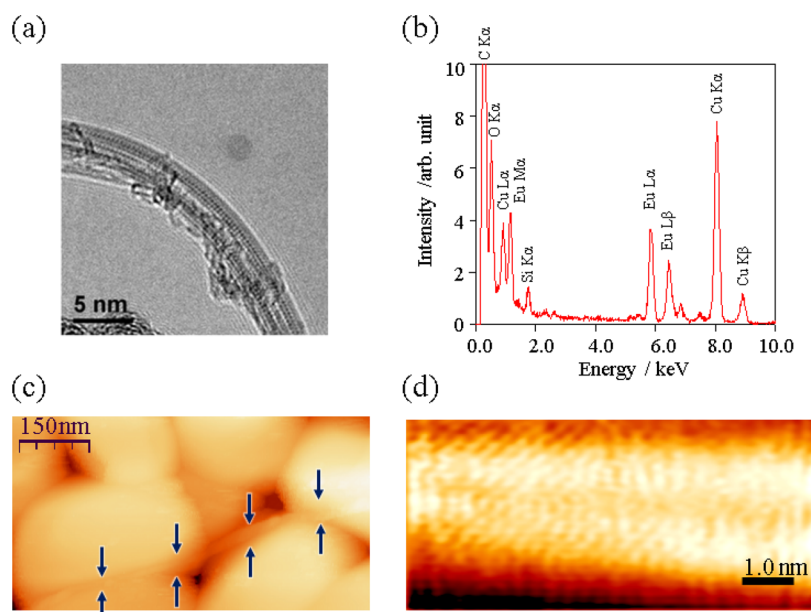


Figure 1. (a) High magnification TEM images of EuNW@CNTs. (b) EDX spectra of EuNW@CNTs. (c) STM image of EuNW@CNTs dispersed in Au(111)/mica. A bundle of EuNW@CNTs is in the place sandwiched between the blue arrows. The bias voltage was 1.01 V, and the current set point was 30.3 pA. (d) STM image of the EuNW@CNT bundle. The black hexagonal lines of the CNT are superimposed to indicate the lattice structure. The bias voltage was -98 mV, and the current set point was 72 pA.

the orbital hybridization and local charge transfer between fullerenes and CNTs.^{23,24} On the other hand, metal NW@CNTs may induce much stronger interactions than fullerene peapods due to the large amount of electron doping^{17,18,25,26} derived from the difference in the electronegativity between metals and carbon. Therefore, the strong interaction between NWs and CNTs is expected to cause the change in the electronic structures of NW@CNTs such as Fermi level shift, band gap reduction, and the emergence of localized states in the gap.

Here, the electronic nature of europium nanowires (EuNWs) encapsulated in CNTs (EuNW@CNTs) is investigated by using STM/STS and DFT calculations. The band gaps of EuNW@CNTs modulate between the EuNW encapsulated area and the empty area, in contrast to the semiconducting CNTs, where those are uniform throughout the entire nanotube axes. The electronic structure is strongly modified due to the interactions between EuNWs and CNTs. The electronic modulation of CNTs by encapsulation of EuNWs is identified as a Fermi level shift and band gap shrinking, as well as the appearance of localized states in the gap. Theoretical DFT results for EuNW@CNTs well explain the electronic modulation of the Fermi level shift and the localized states observed experimentally. Strong interaction between EuNWs and CNTs can actually occur due to the large amount of electron doping, and this leads to the electronic band structure modulation.

2. EXPERIMENTAL SECTION

Sample Preparation. SWCNTs (EC1.0, Meijo Nano Carbon Co., Ltd.) were synthesized by the enhanced direct-injection pyrolytic synthesis (e-DIPS) method. The average diameter of the SWCNTs was estimated from high-resolution transmission electron microscopy (HRTEM) observations to be 1.0 nm. A direct nanofilling method was used to synthesize EuNW@CNTs.^{15,16} Prior to the encapsulation of europium

atoms, the SWCNTs were heated in dry air at 823 K for 30 min in an electric furnace to open the ends of the SWCNTs. Open-ended CNTs and ground europium metal powder were placed in a glass tube under an Ar atmosphere. After vacuum heat treatment at 550 K for 1 h, the glass tube was vacuum sealed at 10^{-4} Pa. The glass tube was then heated at 823 K for 2 days in an electric furnace for encapsulation of Eu atoms. The metal encapsulating CNTs were washed with diluted HCl to remove residual metal atoms attached to the outer surface of the CNTs. The CNTs were then dispersed in tetrahydrofuran (THF) with ammonium carbonate²⁷ by sonication for 4 h. After sonication, the dispersion solution was deposited by drop-casting onto Au(111) substrates, which were flame annealed in air and annealed at 400 K in air prior to the deposition.

STM Measurements. The samples were introduced to an ultrahigh vacuum (UHV) environment and degassed at 500 K prior to STM measurements. The STM/STS measurements were conducted using a microscope (Omicron VT-STM and Unisoku LT-STM) in constant current mode operated at 90 K with an electrochemically etched Ni tip (UNISOKU Co., Ltd.). A lock-in detection technique was used to acquire dI/dV curves. WSxM software was used to process the STM images.²⁸

Computational Details. Theoretical calculations for the structural and electronic properties of EuNW@CNTs were also performed. All calculations were performed based on DFT using the Vienna ab initio simulation package (VASP),^{29,30} where the generalized gradient approximation (GGA) of Perdew–Burke–Ernzerhof (PBE) for the exchange–correlation energy was used. To account for the appropriate orbital dependence of the Coulomb and exchange interactions of the spin-polarized Eu 4f states, the GGA+ U method was employed. The Hubbard parameter for the 4f states was set to $U = 6.0$ eV to reproduce the appropriate 4f energy. A plane wave basis set was employed with a cutoff energy of 500 eV. The interactions between the ionic cores and valence electrons were included through the projector augmented wave (PAW) method.³¹ A special pseudopotential for Eu supplied with VASP was

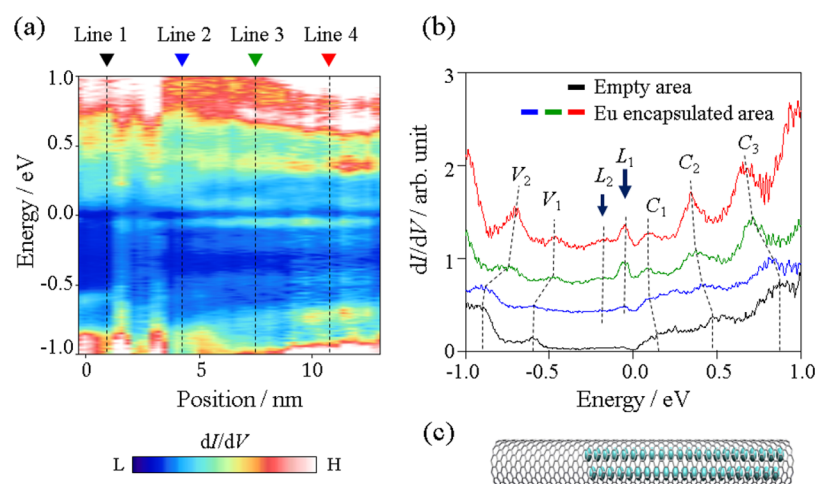


Figure 2. (a) dI/dV mapping of a EuNW@CNT. The horizontal and vertical axes indicate the position along the CNT and the energy, respectively, and the color scale shows the intensity of dI/dV . Modulation amplitude of tunneling voltage is 20 mV, and lock-in frequency is 971 Hz. (b) dI/dV intensity plots for selected vertical line profiles marked by the triangles in (a). The dashed lines indicate the peak position transitions in the STS spectra. Arrows indicate the emerged peaks in the gap area. (c) Structural model of EuNW@CNT that corresponds to (a).

employed. The atomic positions are relaxed with residual forces smaller than 0.03 eV/\AA using a conjugate-gradient algorithm in 20 k -points. One hundred k -points were used for the energy calculation. Europium atoms were placed along the direction of the CNT axis about every 0.42 nm to be commensurate with the periodicity of the CNT and also for simplicity of the calculation.

3. RESULTS AND DISCUSSION

Figure 1a shows a TEM image of EuNW@CNTs. It shows dark areas overlapping with the CNTs in contrast to that of empty CNTs. Figure 1b is the energy dispersive X-ray (EDX) spectrum of EuNW@CNTs, which shows strong peaks of arising from $L\alpha$ and $L\beta$ edges of the Eu atom. Therefore, the dark dots in the CNTs can be assigned to Eu atoms encapsulated in CNTs. The structure of EuNW in Figure 1a exhibits a ladder structure due to their restricted internal space of CNTs.

Figure 1c shows an STM image of EuNW@CNTs dispersed in Au(111)/mica. There is a bundle of EuNW@CNTs in the place sandwiched between the blue arrows. The terrace and step structures of Au(111) are observed. EuNW@CNTs was dispersed in tetrahydrofuran (THF) with ammonium carbonate.²⁷ A small bundle of EuNW@CNTs was deposited on the substrate. Figure 1d shows a corresponding STM image of the bundle of EuNW@CNTs.

A schematic of the CNT lattice structure is superimposed on the image for clarity. This image is taken from the top of a CNT bundle. The chirality index of the bottom CNT was estimated from the image. The chiral angle was measured to be almost 0° , which suggests that these CNTs are of the zigzag type.^{3,4} The width of the CNTs is not clear because they are in a bundle state. The STM image of the bundled EuNW@CNTs is not significantly different from that of an empty CNT at the selected bias.^{3,4} However, the dI/dV curves in Figure 2a show a significant difference between the encapsulated and empty sites of the EuNW@CNTs.

Figure 2a shows dI/dV spectra of EuNW@CNTs used to investigate the effect of EuNW encapsulation. This is the first-time observation of the electronic structure of EuNW@CNTs. The position of the acquired dI/dV spectra is the top of the

bundle, which does not show any change in the features due to topographic modulation. A typical dI/dV spectrum of a CNT at the left side position of the dI/dV mapping area marked by a black triangle in Figure 2a is plotted as the black line in Figure 2b. The dI/dV spectra of the CNT is dominated by van Hove singularities (vHs) derived from the 1D nature of the CNT. The black line in Figure 2b has five vHs peaks. The first vHs peak of the valence band that originates from the CNT is denoted as V_1 , whereas those of the conduction bands are denoted as C_1 , C_2 , and C_3 . In contrast, the other areas of the dI/dV mapping marked by colored triangles in Figure 2a show various features that are not evident along the black triangle line. The dI/dV lines indicated by the blue, green, and red triangles in Figure 2a are shown in Figure 2b with the corresponding colors. The modulated area of the CNT has a different dI/dV line from that of a typical CNT, and its length is greater than 10 nm . A model of the EuNW@CNTs illustrated based on the acquired STS lines is shown in Figure 2c.

The dI/dV spectra for the EuNW@CNTs are significantly modified due to the encapsulation of EuNWs. The peak positions of C_1 – C_3 , V_1 , and V_2 , and the localized states L_1 and L_2 in the dI/dV spectra in Figure 2b are summarized in Table 1. The various Δ values designate the differences between line 1

Table 1. Peak Positions and Peak Shifts in the STS Spectra of EuNW@CNTs

| | line 1 (eV) | line 2 (eV) | line 3 (eV) | line 4 (eV) |
|----------------|-------------|-------------|-------------|-------------|
| peak C_3 | +0.89 | +0.82 | +0.70 | +0.66 |
| Δ_{C_3} | 0 | −0.07 | −0.19 | −0.23 |
| peak C_2 | +0.48 | +0.43 | +0.38 | +0.35 |
| Δ_{C_2} | 0 | −0.05 | −0.10 | −0.13 |
| peak C_1 | +0.12 | +0.10 | +0.09 | +0.09 |
| Δ_{C_1} | 0 | −0.02 | −0.03 | −0.03 |
| L_1 | | −0.05 | −0.05 | −0.05 |
| L_2 | | −0.18 | −0.18 | −0.19 |
| peak V_1 | −0.60 | −0.59 | −0.46 | −0.46 |
| Δ_{V_1} | 0 | +0.01 | +0.14 | +0.14 |
| peak V_2 | −0.91 | −0.87 | −0.74 | −0.69 |
| Δ_{V_2} | 0 | +0.04 | +0.07 | +0.22 |

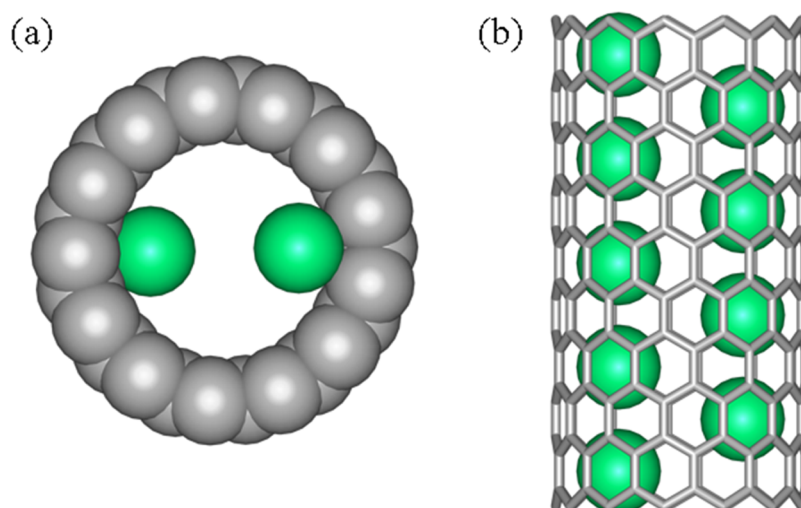


Figure 3. Structural model of geometrically optimized EuNW@CNT: (a) front and (b) side views. The chirality of the CNT is (13,0), the Eu–Eu distance is 0.553 nm, and the periodicity of the unit cell is 0.427 nm. Each unit cell has two Eu atoms.

(empty area) and lines 2–4. For example, C_3 is shifted by -0.23 V (from $+0.89$ to $+0.66$ V) from line 1 to line 4, and V_2 is shifted by $+0.22$ V (from -0.91 to -0.69 V). The STS spectra reveal that the modification of the band structure has three distinctive features. First, the conduction and valence bands shift to the negative direction with respect to the STS spectrum for the empty CNT. C_1 and V_1 are typically symmetric with respect to the Fermi energy, or C_1 is slightly closer to the Fermi level due to electron transfer to the substrate. C_1 is positioned around $+0.1$ eV and V_1 is positioned around -0.6 eV with respect to the Fermi energy in line 2. Second, the difference between C_1 and V_1 decreases at the EuNW encapsulated area. C_1 and V_1 and higher bands are shifted toward the Fermi level. The transitions of peaks are indicated by the dashed lines in Figure 2b. The size of the peak shifts increases in the order of line 4 to line 1. Third, the localized states in the gap, gap states L_1 and L_2 marked by arrows, appear just under the Fermi level. These states are not observed in the empty CNT area, indicating that the localized states are derived from the encapsulation of EuNWs which cause the band modulations.

To obtain further information on the origin of these band modulations, DFT calculations were performed for the bands, DOS, and STS spectra of EuNW@CNTs. For these calculations, the chirality of the CNTs was properly assumed. The observed diameter of the CNT is 1.02 nm, and the dI/dV map shows semiconducting features. Therefore, a (13,0) SWCNT was selected due to its semiconducting properties, in which the computational limitations for the translational vector along the CNT should be small with a fitted diameter to that of EuNWs under periodic conditions. The diameter of the (13,0) CNT is 1.01 nm and the translational vector is 0.427 nm, which is almost comparable to the distance of Eu–Eu obtained from transmission electron microscopy (TEM) observation (0.437 nm).¹⁵ Figure 3 shows the optimized structure of the EuNW@CNTs from DFT simulations. Two atomic rows of Eu were employed because the observed CNT diameter was 1.02 nm. The most probable structure of the EuNW for this diameter CNT is a two-channel staggered structure. The Eu–Eu distance in the unit cell of Figure 3 is 0.553 nm, which is larger than that from TEM observations. The main reason for this difference is the electrostatic repulsion

of positively charged Eu atoms and fixing of the CNT axis length, which is shorter than the observed distance.

Table 2 provides a summary of the results from the DFT calculations, such as the binding energies per number of Eu

Table 2. Number of Eu Atoms per Unit Cell, Binding Energy, Distance of Nearest Neighbor Eu and C, and Charge Transfer from Eu Atoms to CNTs in Current and Previous Work¹⁸

| | n^a | E_b^b (eV/n) | $d(\text{Eu}-\text{C})^c$ (nm) | Q^d (e) |
|--|-------|----------------|--------------------------------|-------------------|
| Eu ₂ @CNT(13,0) | 2 | -1.024 | 0.283 | 1.57 ^e |
| Eu ₁ @CNT(10,0) ¹⁸ | 1 | -1.62 | 0.273 | 1.6 ^f |

^a n is the number of Eu atoms per unit cell. ^b E_b is the binding energy of Eu atoms. ^c $d(\text{Eu}-\text{C})$ is the distance between nearest-neighbor Eu atoms and C atoms. ^d Q is the amount of charge transfer from Eu atoms to CNTs. ^eBader charge analysis was used to calculate the amount of charge transfer from EuNW to CNTs. ^fMulliken population analysis was used for calculating the amount of charge transfer from EuNW to CNTs in previous work.¹⁸

atoms, the nearest Eu–C distance, and charge transfer from Eu atoms. Eu₂@CNT contains two Eu atoms per unit cell calculated in this work, whereas Eu₁@CNT contains one Eu atom per unit cell calculated in a past work.¹⁸ The binding energy of Eu atoms encapsulated in a CNT can be defined as

$$E_b = (E_{\text{tot}} - E_{\text{Eu}} - E_{\text{CNT}})/n \quad (1)$$

where E_{tot} represents the total energy of the EuNW@CNT, E_{Eu} and E_{CNT} are the total energies of an isolated EuNW and pristine CNT, respectively, and n is the number of Eu atoms per unit cell. The binding energy per Eu atom is -1.024 eV, which is exothermic and implies strong interaction between the EuNW and CNT. In previous calculations, E_b was -1.62 eV for the Eu₁@(10,0) CNT system.¹⁸ The difference between these two results is the number of Eu atoms. In the present calculations, the unit cell contains two Eu atoms, and the electrostatic repulsion from two Eu atoms decreases the binding energy.

The binding energy of Eu₂@CNT with an encapsulated NW is -2.048 eV per unit cell, which is slightly larger than that for a fullerene peapod. In previous calculations for C₆₀ fullerene

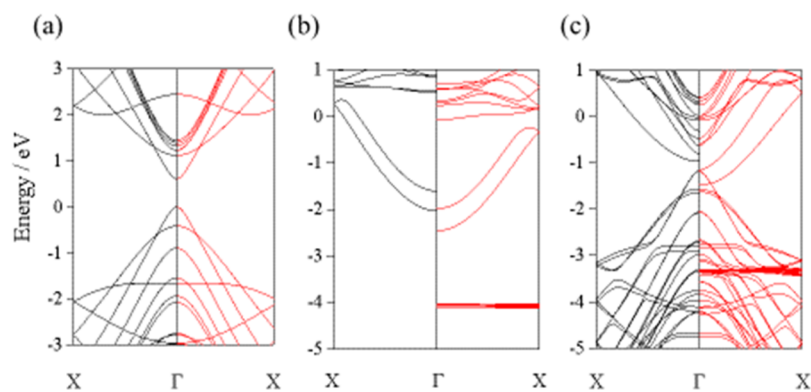


Figure 4. Band structures of (a) pristine (13,0) CNT, (b) EuNW, and (c) EuNW@CNT. The position of EuNW in (b) is same as that in (c). Red, majority spin; black, minority spin.

peapods, the binding energies of C_{60} were -1.61 and -0.51 eV for a (17,0) CNT²⁴ and (10,10) CNT,²³ respectively. Both charge transfer from the fullerene to CNT and orbital hybridization of the lowest unoccupied molecular orbital (LUMO) state of the CNT conduction band are important for the observed band modulation in the STS spectra. The large binding energy in $Eu_2@CNT$ originates not only from van der Waals interactions but also from charge transfer and orbital hybridization.

The large charge transfer causes strong interaction between EuNWs and CNTs. Bader charge analysis³² was used to calculate the charge transfer from the EuNW to CNT in EuNW@CNTs. The total charge from the EuNW that contains two Eu atoms in the CNT is determined to be $+1.57$ e. In a previous study,¹⁸ the charge transfer from $Eu_1@CNT(10,0)$ is $+1.6$ e per Eu atom using Mulliken population analysis. The total amount of charge transfer is almost the same in these two results, suggesting that the magnitude of interaction between Eu atoms and the CNT in these two systems is of the same degree.

Figure 4 shows a band diagram for a pristine (13,0) CNT, an intact EuNW, and an EuNW@CNT. The Eu atom position in the EuNW is the same as that for the structure encapsulated in the CNT. The EuNW is metallic and the band crosses the Fermi energy, whereas the (13,0) CNT is semiconducting with a band gap of 0.61 eV. Figure 4c shows that the bands of the CNT are negatively shifted due to the electron transfer from EuNW in consistency with the charge analysis results. By comparing the band structures of the pristine CNT, intact EuNW, and EuNW@CNT, the rigid filling approximation remains invalid due to the interaction between the EuNW and (13,0) CNT. The entire band shift toward the negative direction in the STS spectra should be represented in the calculation.

To compare the observed STS spectra and band structure, and to determine what bands influence the experimental STS spectra, the partial DOS (PDOS) plot of the EuNW@CNT was examined. Figure 5a shows atom- and spin-resolved PDOS plots for EuNW@CNT. The Eu 6s bands appear below the Fermi level and this band is indeed hybridized, especially with the Eu 5d and C 2p bands. The DOS peak of the Eu state has a finite DOS of the C state at the same energy level. The C states can easily be detected by the STM tip above the CNT surface. Figure 5b shows an electron density plot of the gap states, where the charge density corresponds to the norm of the wave function. The red lines in Figure 5b show an electron

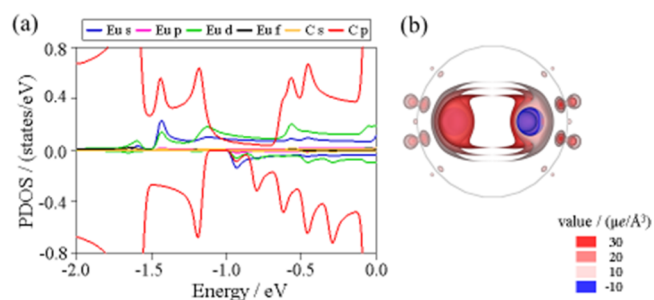


Figure 5. (a) Atom- and spin-resolved partial DOS (PDOS) of EuNW@CNT from -2 to 0 eV. The positive and negative values represent majority and minority spins, respectively. (b) Charge density plots of the gap state at the Γ point. The gap state is around -1 eV. The isosurface values are defined in the color map. The gray circle represents the frame of the CNT.

accumulation contour, and the blue lines show an electron depletion area. Electron density accumulated on the carbon and europium atoms. The electronic states of C atoms can be probed by the STM tip, and the results suggest that Eu encapsulation and orbital hybridization can cause the additional peak in the STS spectrum. The gap states in the STS spectra for the EuNW@CNT emerge upon orbital hybridization of the Eu 6s and 5d states with the C 2p states.

The band gap reduction is qualitatively reproduced in the calculation. The C 2p band, which is the original conduction band before encapsulation, undergoes spin-splitting due to the orbital hybridization with the Eu 6s state. This causes the reduction of the vHs gap. Some higher vHs states do not undergo hybridization with the Eu state, even though all of the peaks in the experimental STS spectra, except for L_1 and L_2 , are shifted. This suggests that the proposed model is still somewhat different from the actual structure and that some electron interactions such as the screening effect³³ are not represented in the calculation.

4. CONCLUSION

Low-temperature STM/STS is used to observe the electronic modulation of CNTs induced by encapsulation of EuNWs, such as a negative band shift, band gap reduction, and the appearance of localized states due to strong EuNW and CNT interactions. DFT calculations well describe the electronic modulation in the Fermi level shift, the change in the localized states by charge transfer from EuNWs to CNTs, and the orbital hybridization of the Eu and C states. The orbital hybridization

of the Eu and C states provides accessible localized states, which can be probed by the STM tip. These observed electronic modulation is attributed to the strong charge transfer interactions exerted between the EuNWs and CNTs.

■ ASSOCIATED CONTENT

Supporting Information

The Supporting Information is available free of charge on the ACS Publications website at DOI: 10.1021/acs.jpcc.7b04047.

STM image of point of STS acquired area; TEM images and EDX of EuNW@CNTs; total energy of EuNW@CNTs as a function of number of k -points; PDOS and simulated STS spectra of EuNW@CNT based on DFT simulations; contour plots of total charge density of EuNW@CNT (PDF)

■ AUTHOR INFORMATION

Corresponding Author

*Tel.: +81-52-789-2482. Fax: +81-52-747-6442. E-mail: noris@nagoya-u.jp.

ORCID

Hidemi Shigekawa: 0000-0001-9550-5148

Hisanori Shinohara: 0000-0001-9400-7622

Notes

The authors declare no competing financial interest.

■ ACKNOWLEDGMENTS

The present study was supported by MEXT/JSPS KAKENHI Grant JP16H06350 and JP25107002.

■ REFERENCES

- (1) Iijima, S. Helical microtubules of graphitic carbon. *Nature* **1991**, *354*, 56–58.
- (2) Saito, R.; Fujita, M.; Dresselhaus, G.; Dresselhaus, M. S. Electronic structure of chiral graphene tubules. *Appl. Phys. Lett.* **1992**, *60*, 2204–2206.
- (3) Wilder, J. W. G.; Venema, L. C.; Rinzler, G. R.; Smalley, R. E.; Dekker, C. Electronic structure of atomically resolved carbon nanotubes. *Nature* **1998**, *391*, 59–62.
- (4) Odom, T. W.; Huang, J.-L.; Kim, P.; Lieber, C. M. Atomic structure and electronic properties of single-walled carbon nanotubes. *Nature* **1998**, *391*, 62–64.
- (5) Smith, B. W.; Monthieux, M.; Luzzi, D. Encapsulated C_{60} in carbon nanotubes. *Nature* **1998**, *396*, 323–324.
- (6) Hirahara, K.; Suenaga, K.; Bandow, S.; Kato, H.; Okazaki, T.; Shinohara, H.; Iijima, S. One-dimensional metallofullerene crystal generated inside single-walled carbon nanotubes. *Phys. Rev. Lett.* **2000**, *85*, 5384–5387.
- (7) Zhao, X.; Ando, Y.; Liu, Y.; Jinno, M.; Suzuki, T. Carbon nanowire made of a long linear carbon chain inserted inside a multiwalled carbon nanotube. *Phys. Rev. Lett.* **2003**, *90*, 187401.
- (8) Nishide, D.; Dohi, H.; Wakabayashi, T.; Nishibori, E.; Aoyagi, S.; Ishida, M.; Kikuchi, S.; Kitaura, R.; Sugai, T.; Sakata, M.; et al. Single-wall carbon nanotubes encaging linear chain $C_{10}H_2$ polyyne molecules inside. *Chem. Phys. Lett.* **2006**, *428*, 356–360.
- (9) Zhao, C.; Kitaura, R.; Hara, H.; Irlle, S.; Shinohara, H. Growth of linear carbon chains inside thin double-wall carbon nanotubes. *J. Phys. Chem. C* **2011**, *115*, 13166–13170.
- (10) Ajayan, P.; Ebbesen, T.; Ichihashi, T.; Iijima, S.; Tanigaki, K.; Hiura, H. Opening carbon nanotubes with oxygen and implications for filling. *Nature* **1993**, *362*, 522–525.
- (11) Meyer, R.; Sloan, J.; Dunin-Borkowski, R.; Kirkland, A.; Novotny, M.; Bailey, S.; Hutchison, J.; Green, M. Discrete atom

imaging of one-dimensional crystals formed within single-walled carbon nanotubes. *Science* **2000**, *289*, 1324–1326.

(12) Philp, E.; Sloan, J.; Kirkland, A.; Meyer, R.; Friedrichs, S.; Hutchison, J.; Green, M. An encapsulated helical one-dimensional cobalt iodide nanostructure. *Nat. Mater.* **2003**, *2*, 788–791.

(13) Li, L.; Khlobystov, A.; Wiltshire, J.; Briggs, G.; Nicholas, R. Diameter-selective encapsulation of metallocenes in single-walled carbon nanotubes. *Nat. Mater.* **2005**, *4*, 481–485.

(14) Kitaura, R.; Ogawa, D.; Kobayashi, K.; Saito, T.; Ohshima, S.; Nakamura, T.; Yoshikawa, H.; Awaga, K.; Shinohara, H. High yield synthesis and characterization of the structural and magnetic properties of crystalline $ErCl_3$ nanowires in single-walled carbon nanotube templates. *Nano Res.* **2008**, *1*, 152–157.

(15) Kitaura, R.; Nakanishi, R.; Saito, T.; Yoshikawa, H.; Awaga, K.; Shinohara, H. High-yield synthesis of ultrathin metal nanowires in carbon nanotubes. *Angew. Chem., Int. Ed.* **2009**, *48*, 8298–8302.

(16) Nakanishi, R.; Kitaura, R.; Ayala, P.; Shiozawa, H.; de Blauwe, K.; Hoffmann, P.; Choi, D.; Miyata, Y.; Pichler, T.; Shinohara, H. Electronic structure of Eu atomic wires encapsulated inside single-wall carbon nanotubes. *Phys. Rev. B: Condens. Matter Mater. Phys.* **2012**, *86*, 115445.

(17) Parq, J. H.; Yu, J.; Kim, G. First-principles study of ultrathin (2×2) Gd nanowires encapsulated in carbon nanotubes. *J. Chem. Phys.* **2010**, *132*, 054701.

(18) Zhou, J.; Yan, X.; Luo, G.; Qin, R.; Li, H.; Lu, J.; Mei, W.; Gao, Z. Structural, electronic, and transport properties of Gd/Eu atomic chains encapsulated in single-walled carbon nanotube. *J. Phys. Chem. C* **2010**, *114*, 15347–15353.

(19) Hornbaker, D. J.; Kahng, S.-J.; Misra, S.; Smith, B. W.; Johnson, A. T.; Mele, E. J.; Luzzi, D. E.; Yazdani, A. Mapping the one-dimensional electronic states of nanotube peapod structures. *Science* **2002**, *295*, 828–831.

(20) Ohashi, K.; Imazu, N.; Kitaura, R.; Shinohara, H. Irregular modulation of density-of-states of nano-peapods encapsulating Gd@ C_{82} metallofullerenes. *J. Phys. Chem. C* **2011**, *115*, 3968–3972.

(21) Lee, J.; Kim, H.; Kahng, S. J.; Kim, G.; Son, Y. W.; Ihm, J.; Kato, H.; Wang, Z. W.; Okazaki, T.; Shinohara, H.; Kuk, Y. Bandgap modulation of carbon nanotubes by encapsulated metallofullerenes. *Nature* **2002**, *415*, 1005–1008.

(22) Iijima, Y.; Ohashi, K.; Imazu, N.; Kitaura, R.; Kanazawa, K.; Taninaka, A.; Takeuchi, O.; Shigekawa, H.; Shinohara, H. STM and STS studies on the density of states modulation of Pr@ C_{82} and $Sc_3C_2@C_{80}$ binary-metallofullerene peapods. *J. Phys. Chem. C* **2013**, *117*, 6966–6971.

(23) Okada, O.; Saito, S.; Oshiyama, A. Energetics and electronic structures of encapsulated C_{60} in a Carbon Nanotube. *Phys. Rev. Lett.* **2001**, *86*, 3835–3838.

(24) Cho, Y.; Han, S.; Kim, G.; Lee, H.; Ihm, J. Orbital hybridization and charge transfer in carbon nanopeapods. *Phys. Rev. Lett.* **2003**, *90*, 106402.

(25) Derycke, V.; Martel, R.; Appenzeller, J.; Avouris, P. Controlling doping and carrier injection in carbon nanotube transistors. *Appl. Phys. Lett.* **2002**, *80*, 2773–2775.

(26) Kim, S. M.; Kim, K. K.; Duong, D. L.; Hirana, Y.; Tanaka, Y.; Niidome, Y.; Nakashima, N.; Kong, J.; Lee, Y. H. Spectroscopic determination of the electrochemical potentials of n-type doped carbon nanotubes. *J. Phys. Chem. C* **2012**, *116*, 5444–5449.

(27) Matsumoto, K.; Takahashi, T.; Otaki, M.; Jikyo, M. Carbon nanotube complex, carbon nanotube dispersion liquid and method of producing them, carbon nanotube dispersion method, and transparent electrode and method of producing the same. Jpn. Patent 2015-168610A, 2015.

(28) Horcas, I.; Fernandez, R.; Gomez-Rodriguez, J. M.; Colchero, J.; Gomez-Herrero, J.; Baro, A. M. WsXM: a software for scanning probe microscopy and a tool for nanotechnology. *Rev. Sci. Instrum.* **2007**, *78*, 013705.

(29) Kresse, G.; Furthmüller, J. Efficiency of ab-initio total energy calculations for metals and semiconductors using a plane-wave basis set. *Comput. Mater. Sci.* **1996**, *6*, 15–50.

(30) Kresse, G.; Furthmüller, J. Efficient iterative schemes for ab initio total-energy calculations using a plane-wave basis set. *Phys. Rev. B: Condens. Matter Mater. Phys.* **1996**, *54*, 11169–11186.

(31) Kresse, G.; Joubert, D. From ultrasoft pseudopotentials to the projector augmented-wave method. *Phys. Rev. B: Condens. Matter Mater. Phys.* **1999**, *59*, 1758–1775.

(32) Henkelman, G.; Arnaldsson, A.; Jonsson, H. A fast and robust algorithm for bader decomposition of charge density. *Comput. Mater. Sci.* **2006**, *36*, 354–360.

(33) Lin, H.; Lagoute, J.; Repain, V.; Chacon, C.; Girard, Y.; Lauret, J.-S.; Ducastelle, F.; Loiseau, A.; Rousset, S. Many-body effects in electronic bandgaps of carbon nanotubes measured by scanning tunnelling spectroscopy. *Nat. Mater.* **2010**, *9*, 235–238.